IEEE Access
Multidisciplinary | Rapid Review | Open Access Journal

Received December 30, 2019, accepted January 17, 2020, date of publication January 27, 2020, date of current version January 31, 2020.

Digital Object Identifier 10.1109/ACCESS.2020.2969461

An Adaptive Generalized Demodulation Method for Multimedia Spectrum Analysis Is Applied in Rolling Bearing Fault Diagnosis

ZENGQIANG MA[1,2], FEIYU LU[2], SUYAN LIU[1,2], (Member, IEEE), AND XIN LI[1]

[1]State Key Laboratory of Mechanical Behavior and System Safety of Traffic Engineering Structures, Shijiazhuang Tiedao University, Shijiazhuang 050043, China
[2]School of Electrical and Electronic Engineering, Shijiazhuang Tiedao University, Shijiazhuang 050043, China

Corresponding author: Suyan Liu (liusuyan@stdu.edu.cn)

This work was supported in part by the National Natural Science Foundation of China under Grant 11790282, in part by the National Natural Science Foundation of China under Grant 11372199, in part by the Natural Science Foundation of Hebei Province under Grant E2016210104, in part by the Hebei Province 333 Talents Project under Grant A201802004, in part by the Graduate Innovation Funding Program of Hebei Province under Grant CXZZBS2019152, and in part by the 2020 Graduate Innovation Funding Project under Grant YC2020062.

ABSTRACT Research into rolling bearing fault diagnosis methods is of great significance because rolling bearings are a key part of mechanical equipment. The effect of iterative generalized demodulation (IGD) on the demodulation of the fundamental frequency component is obvious in the fault diagnosis of rolling bearings at variable speeds. However, there is a problem; the frequency curve of the demodulation octave frequency component overlaps, and multiple determinations of the bandpass filter parameters produce an artificial error that leads to the misdiagnosis of faults. Therefore, a method for rolling bearing fault diagnosis based on adaptive generalized demodulation (AGD) is proposed. First, the resonance band is intercepted by the fast kurtogram and its envelope results. Second, the adaptive chirp mode decomposition (ACMD) algorithm is used to decompose the envelope signal, the relationship between the time and frequency of the signal is clearly characterized by the form of multimedia pictures, and the instantaneous frequency of each signal component is calculated. Third, the instantaneous frequency is used as the phase function to perform generalized demodulation for each signal component. Last, all the demodulated signals are accumulated, and a fast Fourier transform (FFT) is used to extract the fault's characteristic frequency. The proposed method is compared with IGD by using simulation signals and actual bearing signals collected by sensors under the Internet of Things (IoT). An adaptive diagnosis function is realized through this proposed method at variable speeds. Moreover, the average frequency spectrum identification rate of rolling bearing faults is improved by more than 2.6 times compared with that of the IGD in the simulation signal verification and by more than 1.7 times compared with that of the IGD in the real signal verification. This method is strongly immune to noise.

INDEX TERMS Fault diagnosis, rolling bearing, adaptive generalized demodulation, Internet of Things, multimedia.

I. INTRODUCTION

In the mechanical, chemical, energy, and electric power industries, rolling bearings are the most widely used component. Rolling bearings operate under variable speed conditions and bear large loads of mechanical equipment. Most failures in mechanical equipment are caused by rolling bearings; therefore, research on rolling bearing fault diagnosis under variable speeds is extremely important in engineering applications.

Research into mechanical fault diagnosis methods under variable speeds has become a hot spot in recent years [1], [2]. The research is mainly divided into two categories. The first category is bearing fault diagnosis technology based on order tracking, which is recognized as the most effective method [3]; the core idea is signal resampling in the angular domain to obtain a cyclically stable signal [4]. However, this method usually requires the installation of an additional

The associate editor coordinating the review of this manuscript and approving it for publication was Dapeng Wu.

key-phase device to obtain the actual speed, which is difficult to implement in the case of an inconvenient installation. In addition, the key-less phase order tracking technology is used to directly extract the speed curve from the time domain signal, and this curve is used as the phase signals for order tracking to achieve the extraction of order components. However, problems, such as envelope distortion and phase signal estimation accuracy, will occur during the resampling process, which easily leads to errors in the diagnosis results [5], [6], and even can cause a misjudgment of the results. The other category is bearing fault diagnosis technology based on time-frequency analysis. This category abandons the traditional order analysis technology and avoids the problem of low calculation efficiency caused by solving higher-order equations by resampling [7]. Time-frequency analysis is a technology that comprehensively describes the change in a signal's frequency with time and has inherent advantages in analyzing vibration signals of mechanical equipment with variable speed conditions. Commonly used time-frequency analysis methods include short-time Fourier transform, synchronous compression transform, etc. [8], [9]. However, the above two algorithms have flaws related to their insufficient time-frequency resolution and poor adaptive ability in the signal analysis of variable speed bearings.

Generalized demodulation [10] is a method that can transform a nonlinear and nonstationary signal into a linear and stationary signal and can significantly improve the time-frequency resolution of the signal. In the time-frequency spectrum, the curve is straightened to a horizontal straight line. Many scholars have applied this method to the diagnosis of rotating machinery and equipment faults [11], [12]. To determine that the generalized demodulation algorithm is suitable for single-component signals and can easily produce time-frequency curve crossings for multicomponent signals, reference [13] proposed iterative generalized demodulation (IGD). However, iterations need to be repeatedly implemented using a bandpass filter. The higher the number of iterations is, the more human error will be introduced. In addition, the lack of self-adaptability and low diagnostic accuracy limit the application of IGD for practical engineering. Therefore, this paper proposes an adaptive demodulation algorithm for the problems of insufficient adaptive capability and inadequate diagnostic accuracy for rolling bearing fault diagnosis at variable speeds.

Adaptive chirp mode decomposition (ACMD) is a fully adaptive decomposition algorithm [14], [15]. ACMD has broad application prospects for multicomponent emphasized frequency signals and is very suitable for analyzing mechanical vibration signals under variable speed conditions. ACMD can effectively avoid the errors caused by artificially selecting the parameters of a bandpass filter and largely retains useful components with good adaptive ability. The AGD algorithm proposed in this paper, based on its advantages of adaptive decomposition and high calculation accuracy, combined with the generalized demodulation algorithm, solves the problems of large IGD calculation errors, low spectrum recognition rate, and poor adaptability. This approach enables the signal to be straightened in the horizontal direction when the signal is decomposed so that the rolling bearing fault diagnosis is completed through the spectrum diagram. Based on the simulated signals and actual data collected by sensors in the Internet of Things (IoT) [16], [17], this paper compares AGD with IGD. AGD is better than IGD for its noise immunity and improved spectrum recognition rate.

The main contributions of this paper are as follows: (i) The ACMD algorithm is introduced into the study of rolling bearing fault diagnosis. This algorithm achieves adaptive extraction of multidimensional characteristics of bearing signals and effectively avoids the human errors caused by iteration. (ii) A fault diagnosis sensor network is created, and data are automatically collected by a timing sensor network. Based on the multidimensional features, the fast Fourier transform (FFT) algorithm is used to create a spectrum recognition model for fault diagnosis. (iii) The AGD method is proposed to solve the cross-interference problem of the time-frequency curves of multimedia images in IGD analysis and improves the fault diagnosis accuracy and noise resistance.

The arrangement of the remaining chapters is as follows: the second chapter analyzes the generalized demodulation algorithm and adaptive algorithm for rolling bearing fault diagnosis and discusses the existing problems. The third chapter proposes the adaptive generalized demodulation (AGD) algorithm and introduces the algorithm's implementation steps and principles in detail. The fourth chapter verifies the method proposed in this paper using a simulated signal and actual data. Finally, the fifth chapter summarizes the full text.

II. RELATED WORK

A rolling bearing fault signal with variable speed is nonlinear and nonstationary, rendering traditional signal processing methods ineffective [18]; in addition, the generalized demodulation technique can convert this time-varying frequency signal into a constant-frequency signal and comprehensively describe the characteristics of a bearing fault signal frequency that changes over time. IGD [13] is the main method of researchers, but it cannot adaptively decompose the signal, and it easily causes the problem of overlapping time-frequency curves. Therefore, this paper uses an adaptive decomposition method to decompose the rolling bearing signal and combines the signal with the generalized demodulation algorithm to adaptively extract and model the multidimensional signal features, thus improving the accuracy of rolling bearing fault diagnosis under variable speeds. The following section analyzes the work related to generalized demodulation and adaptive algorithms in detail.

A. RELATED RESEARCH OF GENERALIZED DEMODULATION

Define At a constant speed, the fault frequency presented by a rolling bearing envelope time-frequency diagram has a stable and linear relationship. The fault frequency and its

octave frequency of the rolling bearing have obvious peaks in the FFT spectrum, which is consistent with the operational mechanisms of the failure bearing [3]. However, under variable speeds, the fault characteristic presented in the envelope time-frequency graph is nonstationary and nonlinear, which cannot clearly show a changing fault feature, making it difficult to extract the fault characteristics. The generalized demodulation algorithm can just make up for the defect under variable speeds. By selecting the appropriate phase function, the time-frequency curve in the envelope time-frequency graph is transformed into a horizontal curve parallel to the time axis, which is used to determine the characteristic frequency of the demodulated fault by FFT and complete the fault diagnosis [1].

The type of a bearing fault is analyzed based on massive variable speed vibration signal data collected dynamically and regularly by the sensor. The time-frequency analysis techniques (including short-time Fourier transform [19], synchronous compression transform and other methods [20], etc.) discussed above exist to solve the problem of low time-frequency resolution of the signal in the multimedia map [21]. In the reference [10], the generalized demodulation can convert the signal from nonstationary to stable, which significantly improves the time-frequency resolution of the signal. However, a single generalized demodulation cannot deal with multicomponent rolling bearing signals. Reference [22] applied generalized demodulation to an envelope order spectrum to achieve gear fault diagnosis. Based on the multicomponent signal decomposition method of multiple generalized demodulation [23], the wavelet packet's decomposition capability is used to separate the signal after a single demodulation and loop until all components are separated. This method needs to select the basis function in the wavelet packet, which does not have adaptive performance. Reference [24] proposed combining the generalized demodulation algorithm with the actual speed signal to replace the order tracking angular domain resampling process and solved the computational error and efficiency defects in resampling. However, in practical engineering applications, this method is difficult to apply in environments where it is inconvenient to install the key-phase device for velocity measurements, which limits its application in engineering. Reference [25] realized the extraction of multicomponent signals through multiple bandpass filters, and on this basis, an IGD algorithm was proposed to realize the demodulation of multicomponent signals from bearings and complete the fault diagnosis of planetary gears under variable speeds. However, this method has low diagnostic accuracy and poor adaptive ability.

In practical engineering applications, self-adaptation is very important because it can avoid the errors caused by manual selection of parameters, improve the diagnostic accuracy, reduce the prior knowledge required by engineering personnel, operate efficiently and implement unmanned intervention systems. For this reason, we propose an adaptive algorithm to solve the problem of the poor adaptive ability of generalized demodulation.

B. RELATED RESEARCH OF ADAPTABILITY

Adaptability is an important factor to be considered in rolling bearing fault diagnosis. Adaptive algorithms are widely studied. In the field of rolling bearing fault diagnosis, the typical adaptive algorithms include empirical mode decomposition (EMD) [26], ensemble empirical mode decomposition (EEMD) [27], and variation mode decomposition (VMD) [28]. In reference [29] the Hilbert-Huang transformation was applied to gear fault diagnosis, and the fault type was successfully identified. However, the EMD in the Hilbert-Huang transformation has some defects, such as edge effects, overfitting and mode aliasing. To eliminate the phenomenon of mode aliasing in EMD, reference [30] proposed EEMD by adding white noise to the original signal, which effectively suppressed the phenomenon of mode aliasing. Reference [28] provided a new method, VMD, which could simultaneously eliminate EMD mode aliasing and overfitting defects and accelerate the iteration speed. In reference [31], VMD was used to diagnose the fault type of rolling bearings in a multistage centrifugal pump, and good results were obtained. However, there are still some problems in VMD. The endpoint effect still exists after signal decomposition, and the phenomenon of mode aliasing still exists when the frequency conversion rate is fast.

Reference [14] proposes that ACMD has a strong adaptive signal decomposition capability and can decompose multicomponent signals into multiple single-component signals. Different from VMD, ACMD can excavate multicomponent signals separately, retaining the original characteristics of the signals. This approach effectively avoids modal aliasing and can be successfully applied to the diagnosis of faults in rotor-stator systems, effectively identifying the characteristic frequency and multiplier of the fault [14]. Reference [32] applies ACMD to fault diagnosis in variable-speed planetary gears, solving the problem of difficult to extract feature components of complex gearboxes and effectively identifying gear faults. Yang *et al.* [33] mentioned many parameter improvement methods for variational nonlinear chirp mode decomposition (VNCMD) in the time-frequency analysis review and proved their effectiveness and engineering usability. Therefore, based on the advantages of the ACMD algorithm, this paper uses ACMD in the generalized demodulation algorithm for rolling bearing fault diagnosis and proposes the AGD algorithm.

With the development of IoT technology and improved computer hardware performance, data-driven analysis has become a new hot topic in research. This approach does not require prior knowledge of signal processing by engineers and can perform adaptive feature extraction. In terms of data extraction, references [34], [35], [36] focused on reducing the overhead of IoT communication. References [37], [38], [39] contributed to promoting the deployment of the IoT, enhancing knowledge sharing of the IoT and reducing the amount of computing and energy consumption of the IoT. References [40], [41] provided new ideas for massive data analysis based on the IoT and effectively improved the

performance of data cache systems. In this paper, a sensor is used to automatically collect vibration information from variable speeds of a rolling bearing to achieve adaptive multidimensional feature data extraction.

In conclusion, the AGD method solves the problems of poor adaptive ability and low diagnostic accuracy of IGD at variable speeds. First, the multidimensional features of the signal are extracted based on the adaptive algorithm, and the instantaneous frequency of each feature is calculated. Second, according to the generalized demodulation algorithm, the variable speed signal data, which is automatically collected by the sensor at a fixed time, is created to identify the spectrum for the fault diagnosis. Finally, we determine the fault type by observing the multimedia spectrum and calculate the spectrum recognition rate to analyze the fault diagnosis accuracy of the AGD algorithm.

III. THE PROPOSED AGD METHOD

IGD is based on a single-component signal and introduces the idea of iteration and intercepting the generalized demodulated target component through a bandpass filter. The above process is repeated to demodulate the entire multicomponent signal.

However, IGD ignores an important factor, which is that generalized demodulation is derived from a single-component signal. For fault bearing signals whose time-frequency distribution curves are not parallel to each other, the signal after each iteration can appear between components with mixing distortion, causing the phenomenon of spectral aliasing. Meanwhile, selecting the parameters of the bandpass filter multiple times will increase human error, reduce the adaptive performance and accuracy, and relies on the prior knowledge of the engineering staff in the engineering application, which leads to poor adaptability and low diagnostic accuracy. To solve these problems, this paper introduces the ACMD algorithm [14] into the generalized demodulation algorithm to realize adaptive extraction of multidimensional features of variable speed rolling bearing vibration signals. A new fault diagnosis method is proposed to make it more suitable for practical engineering applications and to improve the accuracy and noise immunity of fault diagnosis.

A. THE ACMD PRINCIPLE

ACMD is a processing method for multicomponent strong frequency modulated signals; the ACMD aims at the multicomponent time-varying characteristics of rolling bearing fault signal under variable speeds, and it can analyze the signal components and extract them into multidimensional features [14]. This algorithm can adaptively decompose the signal into multiple single-component signals while retaining the original signal components, achieving nondestructive decomposition of the signal, which effectively avoids modal aliasing and improves diagnostic accuracy. Therefore, this paper applies ACMD to the analysis of rolling bearing fault diagnosis.

First, let $s(t)$ be the rolling bearing vibration signal, where $s(t)$ contains K signal components. Therefore, the signal can be rewritten as:

$$s(t) = \sum_{i=1}^{K} s_i(t) = \sum_{i=1}^{K} A_i(t)\cos(2\pi \int_0^t f_i(\tau)\, d\tau + \theta_i) \quad (1)$$

In this formula, $A_i(t) > 0, f_i(t) > 0$ and θ_i represent the instantaneous amplitude (IA), instantaneous frequency (IF), and initial phase of the i-th signal component, respectively. With signal demodulation technology, formula (1) is rewritten into formula (2)

$$s(t) = \sum_{i=1}^{K} a_i(t)\cos(2\pi \int_0^t f_i^{\%}(\tau)d\tau) + b_i(t)\sin(2\pi \int_0^t f_i^{\%}(\tau)d\tau) \quad (2)$$

where $f_i^{\%}(t)$ is a frequency function of the demodulation operators $\sin(2\pi \int_0^t f_i^{\%}(\tau)d\tau)$ and $\cos(2\pi \int_0^t f_i^{\%}(\tau)d\tau)$. $a_i(t)$ and $b_i(t)$ are the corresponding demodulated signals.

$$\begin{cases} a_i(t) = A_i(t)\cos(2\pi \int_0^t (f_i(\tau) - f_i^{\%}(\tau))d\tau + \theta_i) \\ b_i(t) = -A_i(t)\sin(2\pi \int_0^t (f_i(\tau) - f_i^{\%}(\tau))d\tau + \theta_i) \end{cases} \quad (3)$$

The instantaneous amplitude is $A_i(t) = \sqrt{a_i^2(t) + b_i^2(t)}$, and the instantaneous frequency is $f_i(\tau) - f_i^{\%}(\tau)$. Using a greedy search algorithm, ACMD estimates the signal components one by one. For the i-th signal component:

$$\min_{a_i(t), b_i(t), f_i^{\%}(t)} \{\left\|a_i''(t)\right\|_2^2 + \left\|b_i''(t)\right\|_2^2 + \alpha \left\|s(t) - s_i(t)\right\|_2^2\} \quad (4)$$

Simultaneously,

$$s_i(t) = a_i(t)\cos(2\pi \int_0^t f_i^{\%}(\tau)d\tau) + b_i(t)\sin(2\pi \int_0^t f_i^{\%}(\tau)d\tau) \quad (5)$$

$\|s(t) - s_i(t)\|_2^2$ is a redundant signal after removing the current estimated signal component. For discrete signals at time $t = t_0, L, t_{N-1}$ (N is the number of sampling points). Formula (4) can be rewritten as:

$$\min_{\mathrm{u}_i, f_i} \{\|\Theta \mathrm{u}_i\|_2^2 + \alpha \|s - G_i \mathrm{u}_i\|_2^2\}, \quad \mathrm{u}_i = [\mathrm{a}_i^T, \mathrm{b}_i^T]^T \quad (6)$$

In the formula (6) $\mathrm{a}_i = [a_i(t_0), L, a_i(t_{N-1})]^T$, $\mathrm{b}_i = [b_i(t_0), L, b_i(t_{N-1})]^T$ and $\Theta = \begin{bmatrix} \Omega & \\ & \Omega \end{bmatrix}$, where Ω is a second-order difference matrix. Through the component-by-component decomposition of the signal $s(t)$, the multidimensional features of the vibration signal are accurately extracted.

B. THE AGD METHOD

The AGD method proposed in this paper is an algorithm for diagnosing rolling bearing faults. First, the multidimensional characteristics of the signal are adaptively extracted. Second, generalized demodulation transformation is performed on multiple components to sum up the demodulation results.

Finally, the spectrum recognition model of fault diagnosis is presented by means of multimedia visualization to complete the fault diagnosis of rolling bearings. This method solves the error caused by selecting the parameters of the bandpass filters in the IGD algorithm and improves the accuracy of fault diagnosis and enhances the noise resistance. The AGD method is executed as follows:

Step 1: Multimedia visual analysis of the vibration signal data automatically collected by the sensor at regular intervals. The vibration signal is filtered by a fast kurtogram, and the signal resonance band is selected from it. A Hilbert transform is applied to the resonance band signal, and the signal is interpreted as an envelope signal.

Step 2: The algorithm in Section III part A is used to adaptively extract the multidimensional feature signals from the envelope signal, the first signal component obtained by the curve extraction algorithm is used to calculate the instantaneous frequency, and the speed frequency is the result of the instantaneous frequency divided by the fault characteristic coefficient.

Step 3: Take the speed frequency obtained in step 3 as the phase function and perform the generalized demodulation transformation for the extracted multidimensional signal components, where the phase function of the K component is equal to the product of the speed frequency and K.

Step 4: Accumulate and sum the multidimensional features after demodulation, perform FFT based on the multidimensional features, create a fault diagnosis spectrum identification model, and then determine the fault type from the spectrum diagram to complete the fault diagnosis.

According to Fig. 1, the detailed steps of the method are shown below:

(1) The resonance band of the original signal $x(t)$ is determined by the fast kurtogram filter and design filters $h_1(t)$ and $h_0(t)$:

$$\begin{cases} h_1(t) = h(t)\, e^{j3\pi t/4} & (f \in [0, 1/4]) \\ h_0(t) = h(t)\, e^{j3\pi t/4} & (f \in [1/4, 1/2]) \end{cases} \tag{7}$$

$x(t)$ is filtered several times by $h_1(t)$ and $h_0(t)$, and the kurtosis value of each filtering result is repeatedly calculated

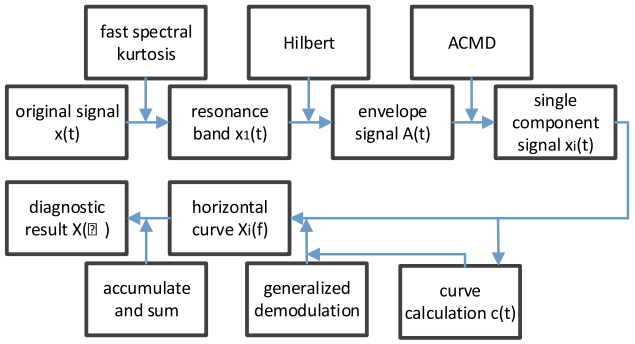

FIGURE 1. The frame diagram of the AGD algorithm.

by the following formula:

$$k = \frac{E\left\langle \left| c_k^i(t) \right|^4 \right\rangle}{\left\{ \left\langle \left| c_k^i(t)^2 \right| \right\rangle \right\}^2} - 2 \quad \left(i = 0, 1, \cdots, 2^k - 1 \right) \tag{8}$$

By accumulating the above kurtosis values, a fast kurtosis graph is constructed, and the resonance band signal with the deepest color in the multimedia graph is intercepted as $x_1(t)$.

(2) The resonance band signal is processed by envelopment analysis. The analytical signal of $x_1(t)$ is calculated by

$$y_1(t) = x_1(t) + jH(x_1(t)) \tag{9}$$

where $H(x_1(t))$ is the Hilbert transform of $x_1(t)$. $y_1(t)$ is then used to calculate the signal envelope as

$$A(t) = \sqrt{y_1(t)^2 + H(y_1(t))^2} \tag{10}$$

(3) The enveloped signal is analyzed by the algorithm in Section III part B, and the instantaneous frequency curve of the single component signal is estimated. The specific steps are as follows:

First, the peak search algorithm [42] is used to calculate the local peak value, and formula (11) is the peak calculation formula

$$\begin{cases} IFE(n_1, k_1) = \underset{k_0 - p \le k \le k_0 + p}{\arg\max} \{SPEC(n_1, k)\} \\ IFE(n_i, k_i) = \underset{\substack{n = n_{i\pm1} \\ k_{i\pm1} - p \le k \le k_{i\pm1} + p}}{\arg\max} \{SPEC(n, k)\} \end{cases} \tag{11}$$

In the formula (11) $n_i = n_1 \pm 1, n_1 \pm 2, \cdots$; $n_i \in (0, M-1)$ and $k_i \in (0, N-1)$, where M is the number of time lines in the time-frequency grid. N is the number of frequency lines in the time-frequency grid. IFE is the peak search function, and arg max is the parameter when the maximum value of the objective function is taken. SPEC is the corresponding time-frequency map. (n_1, k_1) is the first instantaneous frequency coordinate obtained by the peak search with (n_1, k_0) as the starting point. p is the range of the peak search, and (n_i, k_i) is the instantaneous frequency coordinate of each time result obtained through the peak search.

Next, the instantaneous frequency is calculated at each point according to the following formula (12).

$$f(n_i) = \frac{f_q(n_i)}{q} \tag{12}$$

where $f_q(n_i)$ represents the instantaneous frequency of each point obtained by the peak search. q represents the order of fault characteristics corresponding to the instantaneous frequency. n_i represents the corresponding point in time.

Finally, the discrete instantaneous frequency obtained above is transferred to perform a least squares fit. The polynomial degree is selected according to the instantaneous frequency change trend of each point. Generally, the speed does not change abruptly, and a low-order polynomial fit can be

selected. Taking a quadratic as an example, the fitting formula is as follows:

$$\hat{f}(t) = at^2 + bt + c \tag{13}$$

where t represents time, and $\hat{f}(t)$ represents the fitted instantaneous frequency transfer function. a, b, and c are undetermined coefficients. The square error formula is as follows:

$$F(a, b, c) = \sum_{i=1}^{M} [\hat{f}(t_i) - \hat{f}(n_i)]^2 \tag{14}$$

We determine a, b, and c according to $\frac{\partial F}{\partial a} = 0$, $\frac{\partial F}{\partial b} = 0$, $\frac{\partial F}{\partial c} = 0$. Finally, the instantaneous frequency curve $c(t)$ function is fitted.

(4) The AGD algorithm combines the fault characteristic coefficient of the rolling bearings and the instantaneous frequency $c(t)$ to calculate $s_i(t)$, where $s_i(t)$ is the i-th phase function of $x_i(t)$.

$$s_i(t) = \frac{c(t)i}{\delta} \tag{15}$$

δ is the fault characteristic coefficient.

(5) Formula (16) is the result of generalized demodulation of each signal components by using phase function.

$$X_i(f) = \int_{-\infty}^{\infty} x_i(t) e^{-2\pi j[f + s_i(t)]} dt \tag{16}$$

In the multimedia time-frequency diagram, the signal component curves are parallel to the time axis in the time domain. f represents the instantaneous frequency fault point, which can take the ordinate of the initial point of the curve in the actual project.

(6) The summation result is the summation of the demodulated component signals. The summation formula is expressed as

$$X(f) = \sum_{i=1}^{K} X_i(f) \tag{17}$$

(7) Next, we perform FFT on the accumulated result to obtain the spectrum identification model and the final spectrum diagram. The formula is expressed as

$$X(\omega) = \sum_{n=0}^{N-1} x(n) W_N^{nk} \tag{18}$$

In formula (18) the $k = 0, 1, \cdots N-1$, $W_N = e^{-j\frac{2\pi}{N}}$, and $x(n) = X(f)$. By observing the peak value of each component in the multimedia spectrum diagram, we extract the fault features and achieve the fault diagnosis.

IV. EXPERIMENT ANALYSIS

In this paper, the AGD algorithm is compared with the IGD algorithm, and the actual data based on the simulation data are compared with the actual conditions. In the comparison part of the bearing simulation data, signal data are generated through a simulation model of rolling bearing faults that has been proposed in the literature [43], and simulated fault bearing signals under two working conditions are designed to compare and verify the spectral recognition rate and noise resistance of the algorithm under different signal to noise ratios (SNR). For the actual signal component, the equipment is a rotating machinery vibration and fault simulation test bench QPZZ - II. The fault signal of the outer ring of the rolling bearing is selected for comparative verification. The vibration signal is collected by the network sensor, and the spectrum recognition rate of the algorithm is compared and verified.

A. SIMULATION SIGNAL ANALYSIS OF FAULT BEARING

First, the accuracy of the algorithm must be verified according to reference [43] to generate a fault bearing simulation signal.

$$x(t) = \sum_{m=1}^{M} L_m e^{-\beta(t-t_m)} \sin[\omega_r(t - t_m)] u(t - t_m) + n(t) \tag{19}$$

here M is the number of impulse responses, L_m is the m-th impulse response amplitude coefficient, T_p is the response period, β is the structural attenuation coefficient, ω_r is the natural damping coefficient of the system, $u(t)$ is the unit step function, $n(t)$ is Gaussian white noise, and t_m is the time when the m impulse occurs, whose formula is:

$$\begin{cases} t_1 = (1 + \mu)[1/f_c(0)] \\ t_m = \\ (1 + \mu)[1/f_c(0) + 1/f_c(t_1) + \ldots + 1/f_c(t_{m-1})] \\ m = 2, 3, \ldots, M \end{cases} \tag{20}$$

where μ is the error caused by each fault impulse interval with a value generally from $0.01 \sim 0.02$, $f_c = \delta f_r$ is the fault characteristic frequency, f_r is the bearing rotation frequency, and δ is the fault characteristic coefficient. The specific parameter values are shown in Table 1.

TABLE 1. Simulation parameter values of fault bearing.

Speed curve function	20+3 × t	-9.6 × t^2+28.8 × t+58.4
Duration	10 s	3s
Speed change range	20-50 Hz	58.4-80 Hz
Resonance frequency	4000 Hz	4000 Hz
Sampling frequency	20 kHz	20 kHz
Fault characteristic coefficient	3.5	3.5
Attenuation coefficient	500	500
Signal to noise ratio(SNR)	8	8

1) LIFTING SPEED SIMULATION ANALYSIS

We design a set of speed-up simulation signals to test the performance of the algorithm under ramp-up conditions. The speed selection refers to the empirical value of the actual working conditions and is defined as $20 + 3t$. Table 1 shows the specific parameters. Finally, the simulation signal is generated as shown in Fig. 2 (a). The signal amplitude increases with time, and the pulse impact interval decreases.

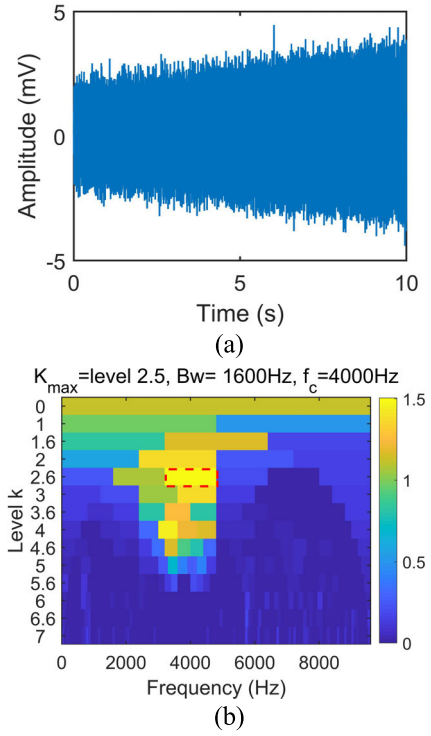

FIGURE 2. The signal preprocessing results for the simulated signal: (a) Time domain diagram of a simulated signal; (b) Fast kurtogram results of simulated signals.

In the simulation analysis, the number of extraction curves is 3. The signal is preprocessed according to the first step of the algorithm proposed in Section III part B, and the simulated signal is subjected to a fast kurtogram filtering algorithm to intercept signals with bright colors. The area shown by the red box (3200 Hz $\sim$ 4800 Hz) in Fig. 2 (b), forms the resonance band signal and obtains the envelope of the resonance band signal.

The multimedia time-frequency diagram of the envelope signal is shown in Fig. 3 (a). The arrows indicate 1-3 times the characteristic frequency of the fault, which are 70 Hz, 140 Hz, and 210 Hz. Next, the adaptive algorithm mentioned in the step 2 of Section III part B is used to extract the multidimensional features of the envelope signal, as shown in Fig. 3 (b). The remaining signal components after decomposing the first component in Fig. 3 (c), and according to the step 3 in Section III part B, the instantaneous frequency curve function of the simulated signal is solved, as shown in Fig. 3 (d). The fault characteristic frequency and fault characteristic coefficient of the simulation signal are combined

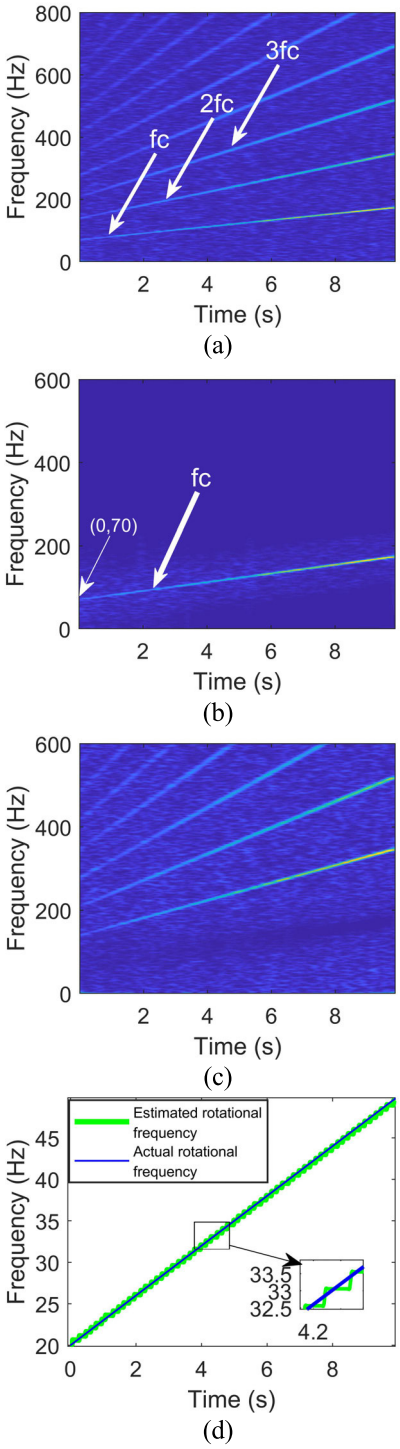

FIGURE 3. Multidimensional feature signal extraction: (a) envelope time-frequency diagram; (b) the first component decomposed; (c) time-frequency diagram after decomposing the first component; (d) comparison of the actual rotational frequency and the estimated rotational frequency.

to calculate the instantaneous rotational frequency, and the results are compared with the actual frequency. The phase function $s(t) = 3 \times 3.5 \div 2t^2 = 5.25t^2$ required for demodulation is determined by the estimated instantaneous rotational frequency and the set fault characteristic coefficient 3.5.

The instantaneous frequency fault point $f = 70Hz$ is calculated by the first component decomposed in Fig. 3 (b). Finally, according to step 4 in Section III part B, generalized demodulation is performed on the extracted single-component signal, the demodulation results are accumulated, and the FFT spectrum recognition model is established. The peak value of the spectrum is observed through the multimedia time-frequency diagram and compared with the actual value.

After the above decomposition process, Fig. 4 (a) shows the accumulated results after generalized demodulation for each component. As seen in the figure, the fault characteristic frequency of 1-3 times parallel to the time axis, and the components are well distinguished, establishing the FFT spectrum fault diagnosis model. In Fig. 4 (b), we can see that the multimedia spectrum plots peak at 70.01, 140.2, and 210.3. It can be verified that the characteristic frequency is equal to the frequency multiplied by the characteristic coefficient, which is consistent with the characteristic frequency of the simulation signal $1 \times 20 \times 3.5$, $2 \times 20 \times 3.5$, $3 \times 20 \times 3.5$ (frequency multiplier $\times$ rotational frequency $\times$ failure factor).

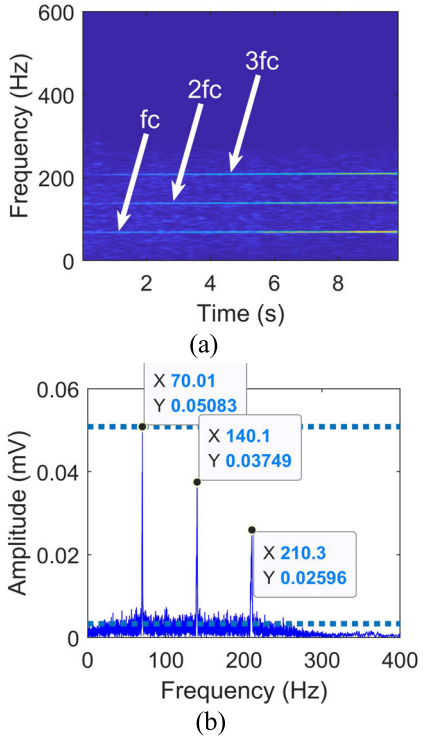

FIGURE 4. The AGD algorithm diagnosis results: (a) accumulated signal after generalized demodulation; (b) FFT spectrogram.

Using the IGD algorithm to compare the method proposed in this article, Fig. 5 (a) shows the effect of the third iteration, which can be seen from the time-frequency diagram. Although the 3 fault characteristic frequency is parallel to the time axis, there are cross interference terms around it. Fig. 5 (b) shows the FFT results after IGD. From the FFT results, it can be intuitively seen that although there is a peak

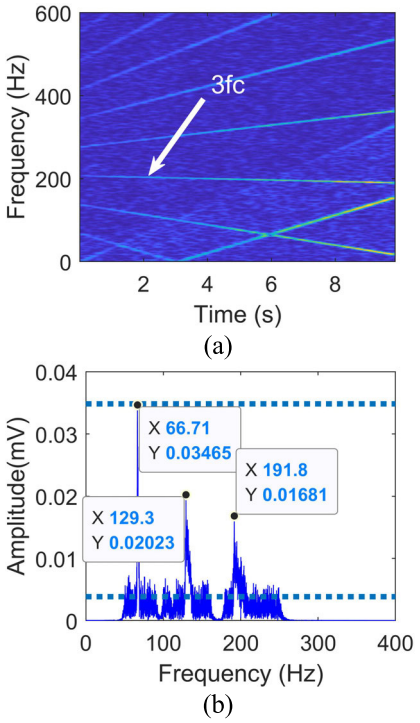

FIGURE 5. The IGD algorithm diagnosis results: (a) time-frequency diagram of the third iteration; (b) FFT spectrogram.

value in the frequency doubling of IGD, the interference term affects the fault diagnosis.

It can be seen from the comparison results of the two pictures in Fig. 4 and Fig. 5 that the IGD exhibits a spectral aliasing phenomenon in the third iteration. The generalized demodulation is insufficient, and the bandpass filter parameters need to be selected multiple times, which increases the influence of manual intervention. The algorithm has poor self-adaptability. The method proposed in this paper successfully avoids the above problems and greatly improves the diagnostic accuracy.

To test the diagnostic accuracy and noise immunity of AGD and to quantitatively measure the accuracy of the method proposed in this paper, the fault diagnosis accuracy was measured under the same signal with a different SNR. According to reference [44], this paper defines the frequency spectrum recognition rate of rolling bearing fault diagnosis as:

$$\rho = \frac{MAX\{\text{Spectral curve energy of characteristic frequency}\}}{AVERAGE\{\text{Noise energy}\}} \tag{21}$$

The performance of the proposed method for simulated signals with different SNRs is tested, as shown in Table 2. Six SNR values are taken from -8 dB to 8 dB. In each case, the diagnostic accuracy of AGD is higher than that of IGD. In addition, with increasing SNR, the relative accuracy of both increases, that is to say, the higher the SNR is, the higher the diagnostic accuracy of AGD is. In addition, as the noise intensity increases, the errors of AGD and IGD both increase.

TABLE 2. Spectrum recognition rate.

ρ	AGD	IGD
SNR=8	15.17	9.05
SNR=4	14.36	8.22
SNR=2	12.67	7.5
SNR=0	10.59	4.33
SNR=-4	8.84	2.78
SNR=-8	5.36	1.49

As the SNR increases from -8 dB to 8 dB, the spectrum recognition rate of the AGD algorithm increases from 5.36 to 15.17, but that of the IGD algorithm increases from 1.49 to 9.05. On the other hand, by comparing the data in Table 2, the average relative accuracy is 5.603, that is, the average of the difference between the spectrum identification rates between AGD and IGD under all SNR conditions.

It can be seen from the above analysis that the AGD method is superior to the IGD in terms of noise immunity and that with the same SNR, the spectrum recognition rate is higher than that of the IGD.

2) COMPLEX WORKING CONDITION

To simulate the real bearing signals of complicated conditions, the designed speed function is $-9.6t^2 + 28.8t + 58.4$, and the specified parameters are shown in Table 1. Fig. 6 (a) is the time-frequency diagram of the simulated enveloped signal after calculating the fast kurtogram algorithm. These arrows point to the 1-3 times fault characteristic frequency of the signals. Fig. 6 (b) shows the extracted instantaneous rotational frequency curve after being processed by the third step of the algorithm in Section III part B. The instantaneous frequency and the known fault characteristic coefficient (3.5) determine the phase function, which is applicable to the generalized demodulation. Using the phase function to perform the generalized demodulation transformation on the three components

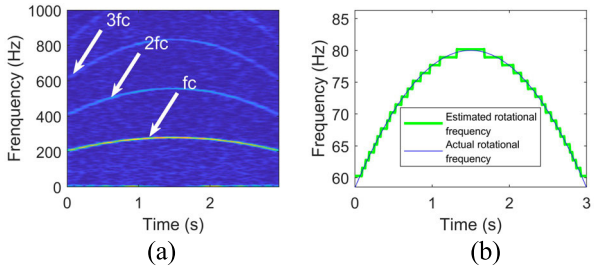

FIGURE 6. The signal envelope and the calculated rotational frequency: (a) the envelope time-frequency diagram obtained by signal preprocessing; (b) the comparison of calculated rotational frequencies.

and accumulating these demodulated components establishes the spectrum identification model of FFT. The spectral peak of the multimedia time-frequency diagram are observed and compared with the actual value.

As shown in Fig. 7 (a), clear peaks appear at 1-3 times the fault characteristic frequency, and there are no interference terms. Fig. 7 (b) shows the results of IGD, and although we can see three clear peaks, there is a significant error in the extracted fault characteristic frequency within 5-30 Hz, which is not acceptable in practical engineering.

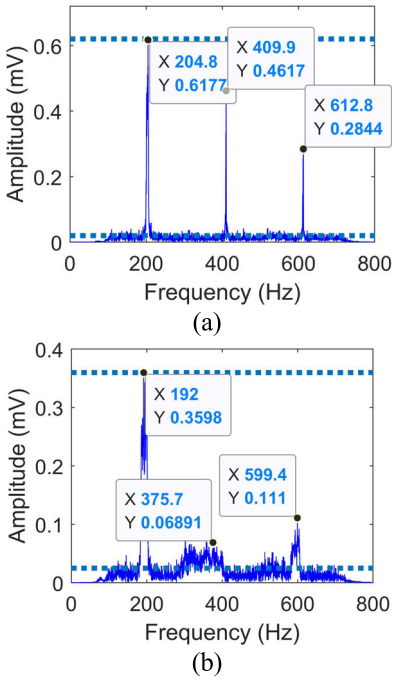

FIGURE 7. The comparison fault diagnosis results between AGD and IGD for a simulated signal: (a) FFT spectrogram of AGD; (b) FFT spectrogram of IGD.

Under the simulated signal of this complex condition, the frequency spectrum recognition rates under different SNRs are shown in Table 3. In each SNR case, the diagnostic accuracy of AGD is higher than that of IGD, and the average relative accuracy is approximately 8.89 times higher. Meanwhile, with increasing SNR, the relative accuracy and diagnostic accuracy of both approaches increase. In addition, with increasing noise intensity, the errors from AGD and IGD increase. When the SNR increases from -8 dB to 8 dB, the frequency spectrum recognition rate of the AGD algorithm increases from 2.11 to 24.32, and the frequency spectrum recognition rate of the IGD algorithm increases from 0.13 to 10.6. It is shown that the noise immunity of the AGD algorithm is better than that of IGD.

The AGD algorithm will extract one component each time, and then perform generalized demodulation for each signal component in turn, which seems to be a cyclic process. In fact, AGD can decompose a single component and make a generalized demodulation transformation of the component, which is essentially a top-down process; this process avoids

TABLE 3. Spectrum recognition rate.

ρ	AGD	IGD
SNR=8	29.52	14.75
SNR=4	20.67	10.2
SNR=2	19.66	7.5
SNR=0	13.59	3.68
SNR=-4	5.79	1.86
SNR=-8	3.17	1.03

the iterative process of the generalized demodulation cycle and effectively solves the problem of multiple selections of bandpass filter parameters, which reduces the diagnosis error and effectively improves the self-adaptability of fault diagnosis.

As the above analysis results fully explain, the fault characteristic frequencies are 3.5 times the actual speed in the two bearing simulation signals, and they contain 1-3 times the fault characteristic frequency fault points. This finding is consistent with the assumptions of the simulation model, which verifies the effectiveness of the AGD algorithm. In addition, the AGD method also has a high-precision spectrum recognition rate when the SNR is less than zero, which improves fault diagnosis accuracy and noise immunity.

B. ACTUAL SIGNAL ANALYSIS OF FAULT BEARING

The feasibility of the AGD method was verified by measuring the fault signals of the outer ring rolling bearing. The equipment used in this paper is a QPZZ-II system of a rotating machinery vibration and fault simulation test bench, as shown in Fig. 8. Fig. 8 (a) uses a sensor with IoT technology to collect vibration signals, and 2 is a laser tachometer for measuring the actual speed. Fig. 8 (b) shows the installation position of the vibration acceleration sensor. The rolling bearing model parameters are shown in Table 4. The bearing outer ring fault characteristic coefficient is 5.284.

TABLE 4. Target bearing parameters.

Bearing type	The number of rolling bodies	Diameter of rolling body	Diameter of pitch circle	Contact-angle α
U205EM	13	7.2 mm	38.5 mm	0

The sampling frequency set in the experiment is 25600 Hz, and the sampling time is 5 s. The two signals from the bearing vibration signal and the laser tachometer are collected separately. The collected vibration signal is shown in Fig. 9 (a). After the fast kurtogram algorithm is applied, the envelope

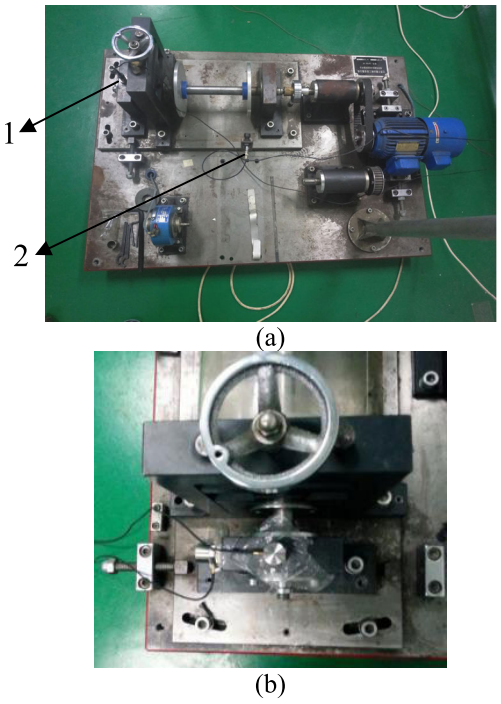

FIGURE 8. Vibration and fault simulation test bench for rotating machinery: (a) simulation experiment platform; (b) installation position of vibration acceleration sensor.

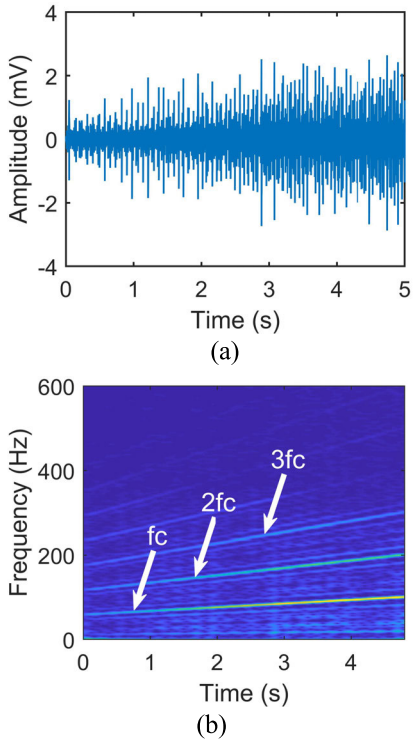

FIGURE 9. The signal preprocessing results for actual signals: (a) time domain diagram of actual signals; (b) envelope time-frequency diagram.

signal is adaptively processed, and the first decomposed signal is used to estimate the rotational frequency. This estimation is compared with the actual rotational frequency measured by the laser tachometer, as shown in Fig. 10. We use the estimated rotational frequency to perform a generalized

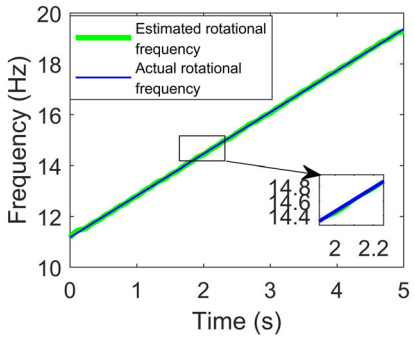

FIGURE 10. Comparison of the actual rotational frequency and the estimated rotational frequency.

demodulation transformation on the corresponding decomposed components, so the curve in the multimedia time-frequency diagram is parallel to the time axis, and then the demodulation results are accumulated and summed up. A spectrum identification model of FFT for the accumulated signal, as shown in Fig. 11 (a). Fig. 11 (b) is the result of the spectrum identification model of IGD. It can be seen from the comparison that the AGD method can more accurately extract 1-3 times the fault characteristic frequency, which are $1 \times 11.4 \times 5.28$, $2 \times 11.4 \times 5.28$, $3 \times 11.4 \times 5.28$ (frequency multiplier $\times$ rotational frequency $\times$ fault factor). The fault spectrum identification rate is $\frac{0.2022}{0.005419} = 37.313$, perfectly fitting the bearing outer ring fault type. The IGD

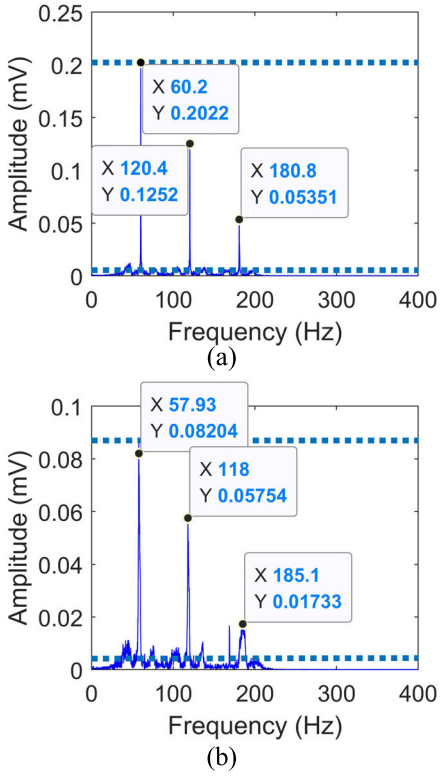

FIGURE 11. The comparison of fault diagnosis results between AGD and IGD for an actual signal: (a) FFT spectrogram of AGD; (b) FFT spectrogram of IGD.

has a 3-5 Hz error in extracting the characteristic frequency of the fault, and there are many interference terms at the third frequency. At this time, the fault spectrum recognition rate is $\frac{0.08698}{0.00419} = 20.76$.

To summarize, the diagnostic accuracy of the AGD method is better than that of the IGD method, which has a good suppression effect on the interference terms and eliminates the repeated selection of the bandpass filter parameters in the iteration process. In the simulation signal verification, the average spectrum recognition rate is increased to 2.6 times that of the IGD, and in the real signal verification, the spectrum recognition rate is increased by more than 1.7 times, which improves the fault diagnosis accuracy of rolling bearings. The noise of the actual signal has been determined. If noise is artificially added, it leads to unreliability in the experimental data. Therefore, in the actual signal section, the noise resistance is not analyzed.

V. CONCLUSION

Based on the advantages of the generalized demodulation and adaptive algorithm, the AGD method is proposed for diagnosing rolling bearing faults at variable speeds. This method solves the demodulation deficiency of IGD by extracting the fault characteristics of rolling bearings, extracting the overlapping fault features, and selecting the bandpass parameters repeatedly. This approach enhances the adaptive ability of the algorithm and improves the recognition rate of the fault spectrum and noise resistance. The study draws the following main conclusions:

(1) Integrating the ACMD algorithm with generalized demodulation and introducing it into the field of rolling bearing fault diagnosis can take full advantage of the generalized demodulation and adaptively perform multidimensional feature extraction of vibration signals. The ACMD signal adaptively decomposes into K components. K is determined by the signal itself and does not need to set parameters manually. This approach solves the problem of the artificial error in the algorithm and has inherent advantages in the preprocessing of rotating machinery signals.

(2) Compared with the IGD algorithm, the method proposed in this paper improves the spectrum recognition rate in the verification processing of simulation signals and real signals, so the fault diagnosis accuracy is higher.

(3) The algorithm is verified based on bearing simulation signals and experimental data. The method proposed in this paper can solve the problem of selecting the parameters of a bandpass filter many times by IGD and effectively avoids the error caused by setting the parameters manually. This approach also improves the noise resistance of the algorithm, which is more suitable for practical engineering applications.

REFERENCES

[1] D. Zhao, J. Li, W. Cheng, and W. Wen, "Multi-fault feature detection of rolling element bearing by an iterative generalized demodulation algorithm under time-varying rotational speed," *J. Vib. Shock*, vol. 37, no. 4, pp. 177–183 and 190, 2018, doi: 10.13465/j.cnki.jvs.2018.04.027.

[2] J. Xia, Z. Wang, C. Chen, Q. Lv, and K. Liu, "Fault feature extraction for rolling bearings based on integrated order-frequency spectral correlation," *J. Vib. Shock*, vol. 37, no. 23, pp. 78–83, 2018, doi: 10.13465/j.cnki.jvs.2018.23.011.
[3] Y. Guo, T.-W. Liu, J. Na, and R.-F. Fung, "Envelope order tracking for fault detection in rolling element bearings," *J. Sound Vib.*, vol. 331, no. 25, pp. 5644–5654, Dec. 2012, doi: 10.1016/j.jsv.2012.07.026.
[4] K. Bossley, R. Mckendrick, C. Harris, and C. Mercer, "Hybrid computed order tracking," *Mech. Syst. Signal Process.*, vol. 13, no. 4, pp. 627–641, Jul. 1999, doi: 10.1016/j.jsv.2012.07.026.
[5] Y. Guo, Y. L. Chi, Y. Y. Huang, and S. R. Qin, "Robust IFE based order analysis of rotating machinery in virtual instrument," in *Proc. J. Phys., Conf.*, vol. 48, pp. 647–652, Oct. 2006, doi: 10.1088/1742-6596/48/1/121.
[6] W. Cheng, T. Wang, J. Wang, and X. Gao Robert, "Effects and its elimination method of envelope deformation on order analysis," *J. Vib. Eng.*, vol. 28, no. 3, pp. 470–477, 2015, doi: 10.16385/j.cnki.issn.1004-4523.2015.03.018.
[7] C. Li, V. Sanchez, G. Zurita, M. C. Lozada, and D. Cabrera, "Rolling element bearing defect detection using the generalized synchrosqueezing transform guided by time–frequency ridge enhancement," *ISA Trans.*, vol. 60, pp. 274–284, Jan. 2016.
[8] W. J. Wang and P. D. McFadden, "Early detection of gear failure by vibration analysis i. calculation of the time-frequency distribution," *Mech. Syst. Signal Process.*, vol. 7, no. 3, pp. 193–203, May 1993, doi: 10.1006/mssp.1993.1008.
[9] C. Li and M. Liang, "Time–frequency signal analysis for gearbox fault diagnosis using a generalized synchrosqueezing transform," *Mech. Syst. Signal Process.*, vol. 26, pp. 205–217, Jan. 2012, doi: 10.1016/j.ymssp.2011.07.001.
[10] S. Olhede and A. Walden, "A generalized demodulation approach to time-frequency projections for multicomponent signals," *Proc. Roy. Soc. A, Math., Phys. Eng. Sci.*, vol. 461, no. 2059, pp. 2159–2179, Jul. 2005, doi: 10.1098/rspa.2005.1455.
[11] H. Li, B. Tang, Y. Han, and L. Deng, "Fault diagnosis of rolling bearing under a variable rotational speed and gear vibration noise based on revised ANC algorithm and FCO spectrum," *J. Vib. Shock*, vol. 37, no. 23, pp. 38–44, 2018, doi: 10.13465/j.cnki.jvs.2018.23.006.
[12] Z. Feng, F. Chu, and M. J. Zuo, "Time–frequency analysis of time-varying modulated signals based on improved energy separation by iterative generalized demodulation," *J. Sound Vib.*, vol. 330, no. 6, pp. 1225–1243, Mar. 2011, doi: 10.1016/j.jsv.2010.09.030.
[13] Z. Feng, X. Chen, M. Liang, and F. Ma, "Time–frequency demodulation analysis based on iterative generalized demodulation for fault diagnosis of planetary gearbox under nonstationary conditions," *Mech. Syst. Signal Process.*, vols. 62–63, pp. 54–74, Oct. 2015, doi: 10.1016/j.ymssp.2015.03.014.
[14] S. Chen, Y. Yang, Z. Peng, S. Wang, W. Zhang, and X. Chen, "Detection of rub-impact fault for rotor-stator systems: A novel method based on adaptive chirp mode decomposition," *J. Sound Vib.*, vol. 440, pp. 83–99, Feb. 2019, doi: 10.1016/j.jsv.2018.10.010.
[15] S. Chen, X. Dong, Z. Peng, W. Zhang, and G. Meng, "Nonlinear chirp mode decomposition: A variational method," *IEEE Trans. Signal Process.*, vol. 65, no. 22, pp. 6024–6037, Nov. 2017, doi: 10.1109/TSP.2017.2731300.
[16] Z. Zhang and L. Wang, "Social tie-driven content priority scheme for D2D communications," *Inf. Sci.*, vol. 480, pp. 160–173, Apr. 2019, doi: 10.1016/j.ins.2018.12.045.
[17] Z. Zhang, C. Wang, C. Gan, S. Sun, and M. Wang, "Automatic modulation classification using convolutional neural network with features fusion of SPWVD and BJD," *IEEE Trans. Signal Inf. Process. Over Netw.*, vol. 5, no. 3, pp. 469–478, Sep. 2019, doi: 10.1109/TSIPN.2019.2900201.
[18] D. Abboud, J. Antoni, S. Sieg-Zieba, and M. Eltabach, "Envelope analysis of rotating machine vibrations in variable speed conditions: A comprehensive treatment," *Mech. Syst. Signal Process.*, vol. 84, pp. 200–226, Feb. 2017, doi: 10.1016/j.ymssp.2016.06.033.
[19] K. Jaganathan, Y. C. Eldar, and B. Hassibi, "STFT phase retrieval: Uniqueness guarantees and recovery algorithms," *IEEE J. Sel. Topics Signal Process.*, vol. 10, no. 4, pp. 770–781, Jun. 2016, doi: 10.1109/JSTSP.2016.2549507.
[20] C. A. Perez-Ramirez, J. P. Amezquita-Sanchez, H. Adeli, M. Valtierra-Rodriguez, D. Camarena-Martinez, and R. J. Romero-Troncoso, "New methodology for modal parameters identification of smart civil structures using ambient vibrations and synchrosqueezed wavelet transform," *Eng. Appl. Artif. Intell.*, vol. 48, pp. 1–12, Feb. 2016, doi: 10.1016/j.engappai.2015.10.005.
[21] G. Yu, M. Yu, and C. Xu, "Synchroextracting Transform," *IEEE Trans. Ind. Electron.*, vol. 64, no. 10, pp. 8042–8054, Oct. 2017, doi: 10.1109/TIE.2017.2696503.
[22] J. Cheng, B. Li, Y. Yang, and D. Yu, "Application of the envelope order spectrum based on the generalized demodulation time-frequency analysis to the gear fault diagnosis," *J. Vib. Eng.*, vol. 22, no. 5, pp. 467–473, 2009, doi: 10.16385/j.cnki.issn.1004-4523.2009.05.017.
[23] J. Cheng, Y. Yang, and D. Yu, "A multi-component signal decomposition method based on the generalized demodulation time-frequency analysis," *J. Vib. Eng.*, vol. 20, no. 6, pp. 563–569, 2007, doi: 10.16385/j.cnki.issn.1004-4523.2007.06.017.
[24] D. Zhao, J. Li, W. Cheng, and W. Wen, "Compound faults detection of rolling element bearing based on the generalized demodulation algorithm under time-varying rotational speed," *J. Sound Vib.*, vol. 378, pp. 109–123, Sep. 2016, doi: 10.1016/j.jsv.2016.05.022.
[25] X. Chen, "Planetary gearbox fault diagnosis under time-variant conditions based on iterative generalized synchro squeezing transform," *J. Mech. Eng.*, vol. 51, no. 1, p. 131, 2015, doi: 10.3901/JME.2015.01.131.
[26] P. Flandrin, G. Rilling, and P. Goncalves, "Empirical mode decomposition as a filter bank," *IEEE Signal Process. Lett.*, vol. 11, no. 2, pp. 112–114, Feb. 2004, doi: 10.1109/LSP.2003.821662.
[27] M. E. Torres, M. A. Colominas, G. Schlotthauer, and P. Flandrin, "A complete ensemble empirical mode decomposition with adaptive noise," in *Proc. IEEE Int. Conf. Acoust., Speech Signal Process. (ICASSP)*, May 2011. pp. 4144–4147, doi: 10.1109/ICASSP.2011.5947265.
[28] K. Dragomiretskiy and D. Zosso, "Variational mode decomposition," *IEEE Trans. Signal Process.*, vol. 62, no. 3, pp. 531–544, Feb. 2013, doi: 10.1109/TSP.2013.2288675.
[29] D. Yu, "Application of Hilbert-Huang transform method to gear fault diagnosis," *J. Mech. Eng.*, vol. 41, no. 6, p. 102, 2005.
[30] Z. Wu and N. E. Huang, "Ensemble empirical mode decomposition: A noise-assisted data analysis method," *Adv. Adapt. Data Anal.*, vol. 01, no. 1, pp. 1–41, Jan. 2009, doi: 10.1142/S1793536909000047.
[31] M. Zhang, Z. Jiang, and K. Feng, "Research on variational mode decomposition in rolling bearings fault diagnosis of the multistage centrifugal pump," *Mech. Syst. Signal Process.*, vol. 93, pp. 460–493, Sep. 2017, doi: 10.1016/j.ymssp.2017.02.013.
[32] S. Chen, M. Du, Z. Peng, Z. Feng, and W. Zhang, "Fault diagnosis of planetary gearbox under variable-speed conditions using an improved adaptive chirp mode decomposition," *J. Sound Vib.*, vol. 468, Mar. 2020, Art. no. 115065, doi: 10.1016/j.jsv.2019.115065.
[33] Y. Yang, Z. Peng, W. Zhang, and G. Meng, "Parameterised time-frequency analysis methods and their engineering applications: A review of recent advances," *Mech. Syst. Signal Process.*, vol. 119, pp. 182–221, Mar. 2019, doi: 10.1016/j.ymssp.2018.07.039.
[34] P. Zhang, X. Kang, X. Li, Y. Liu, D. Wu, and R. Wang, "Overlapping community deep exploring-based relay selection method toward multi-hop D2D communication," *IEEE Wireless Commun. Lett.*, vol. 8, no. 5, pp. 1357–1360, Oct. 2019, doi: 10.1109/LWC.2019.2917907.
[35] P. Zhang, X. Li, Y. Liu, X. Kang, and Y. Liu, "SDU: State-based dual-mode sensor search mechanism toward Internet of Things," *IEEE Access*, vol. 7, pp. 147962–147974, 2019, doi: 10.1109/ACCESS.2019.2946727.
[36] P. Zhang, X. Kang, D. Wu, and R. Wang, "High-accuracy entity state prediction method based on deep belief network toward IoT search," *IEEE Wireless Commun. Lett.*, vol. 8, no. 2, pp. 492–495, Apr. 2019, doi: 10.1109/LWC.2018.2877639.
[37] D. Wu, Z. Zhang, S. Wu, J. Yang, and R. Wang, "Biologically inspired resource allocation for network slices in 5G-enabled Internet of Things," *IEEE Internet Things J.*, vol. 6, no. 6, pp. 9266–9279, Dec. 2019, doi: 10.1109/JIOT.2018.2888543.
[38] D. Wu, B. Liu, Q. Yang, and R. Wang, "Social-aware cooperative caching mechanism in mobile social networks," *J. Netw. Comput. Appl.*, vol. 149, Jan. 2020, Art. no. 102457, doi: 10.1016/j.jnca.2019.102457.
[39] D. Wu, H. Shi, H. Wang, R. Wang, and H. Fang, "A feature based learning system for Internet of Things applications," *IEEE Internet Things J.*, vol. 6, no. 2, pp. 1928–1937, Apr. 2019, doi: 10.1109/JIOT.2018.2884485.
[40] Z. Li, Y. Jiang, Y. Gao, L. Sang, and D. Yang, "On buffer-constrained throughput of a wireless-powered communication system," *IEEE J. Select. Areas Commun.*, vol. 37, no. 2, pp. 283–297, Feb. 2019, doi: 10.1109/JSAC.2018.2872374.
[41] Z. Li, J. Chen, and Z. Zhang, "Socially aware caching in D2D enabled Fog radio access networks," *IEEE Access*, vol. 7, pp. 84293–84303, 2019, doi: 10.1109/ACCESS.2019.2924939.

[42] B. Boashash, "Estimating and interpreting The instantaneous frequency of a signal-part 1: Fundamentals," *Proc. IEEE*, vol. 80, no. 4, pp. 520–538, Apr. 1992, doi: 10.1109/5.135376.
[43] H. Huang, N. Baddour, and M. Liang, "Bearing fault diagnosis under unknown time-varying rotational speed conditions via multiple time-frequency curve extraction," *J. Sound Vib.*, vol. 414, pp. 43–60, Feb. 2018, doi: 10.1016/j.jsv.2017.11.005.
[44] Z. Ma, X. Liu, J. Zhang, and J. Wang, "Application of VMD-ICA combined method in fault diagnosis of rolling bearings," *J. Vib. Shock*, vol. 36, no. 13, pp. 201–207, 2017, doi: 10.13465/j.cnki.jvs.2017.13.032.

ZENGQIANG MA received the Ph.D. degree from Beijing Jiaotong University, China, in 2011.

He is currently the Special Allowance Expert of the Hebei Provincial Government, the second-level talent of the 333 talent project in Hebei, a member of the Steering Committee of Electrical Information Teaching, Hebei Higher Education Institutions, and the Director of Hebei Electrotechnical Society. He is also a Ph.D. Supervisor and the Deputy Dean of the School of Electrical and Electronic Engineering, Shijiazhuang Tiedao University. He mainly researches the field of safety operation state monitoring and fault diagnosis of rail vehicles, takes the fault or damage identification of wheelset bearings, treads, rails, pantographs, catenaries, and other equipment that affect the safety of rail transit vehicles as research directions. His works based on digital signal processing, digital image processing, embedded development and other technologies, carrying out algorithm innovation, system simulation, experimental verification, prototype development, and so on.

FEIYU LU received the B.S. degree from Beihua University, in 2018. He is currently pursuing the M.S. degree with Shijiazhuang Tiedao University. His main research interests include rotating machinery condition monitoring and fault diagnosis.

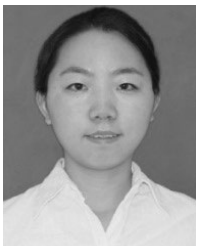

SUYAN LIU (Member, IEEE) received the Ph.D. degree from the Beijing University of Posts and Telecommunications, China, in 2019. She worked as a Software Engineer for Six years and became a Senior Computer Engineer, in 2015. She is currently a Lecturer with the School of Shijiazhuang Tiedao University, China. Her current research interests include machine learning, the Internet of Things, and multimedia image processing technology for fault diagnosis of rolling bearing.

XIN LI received the B.S. degree from Liaoning Shihua University, in 2012, and the M.S. degree from Northeastern University, in 2014. She is currently pursuing the Ph.D. degree with Shijiazhuang Tiedao University. Her main research interests include rotating machinery condition monitoring and fault diagnosis.